Journal of
Biomedical Optics

BiomedicalOptics.SPIEDigitalLibrary.org

Quantification of focal adhesion dynamics of cell movement based on cell-induced collagen matrix deformation using second-harmonic generation microscopy

Yong Guk Kang
Hwanseok Jang
Taeseok Daniel Yang
Jacob Notbohm
Youngwoon Choi
Yongdoo Park
Beop-Min Kim

SPIE.

Yong Guk Kang, Hwanseok Jang, Taeseok Daniel Yang, Jacob Notbohm, Youngwoon Choi, Yongdoo Park, Beop-Min Kim, "Quantification of focal adhesion dynamics of cell movement based on cell-induced collagen matrix deformation using second-harmonic generation microscopy," *J. Biomed. Opt.* **23**(6), 065001 (2018), doi: 10.1117/1.JBO.23.6.065001.

Journal of Biomedical Optics 23(6), 065001 (June 2018)

Quantification of focal adhesion dynamics of cell movement based on cell-induced collagen matrix deformation using second-harmonic generation microscopy

Yong Guk Kang,[a,†] **Hwanseok Jang,**[b,†] **Taeseok Daniel Yang,**[a] **Jacob Notbohm,**[c] **Youngwoon Choi,**[a] **Yongdoo Park,**[b,*] **and Beop-Min Kim**[a,*]
[a]Korea University, Department of Bio-convergence Engineering, Seoul, Republic of Korea
[b]Korea University Medical Center, Department of Biomedical Science, College of Medicine, Seoul, Republic of Korea
[c]University of Wisconsin–Madison, Department of Engineering Physics, Madison, Wisconsin, United States

Abstract. Mechanical interactions of living cells with the surrounding environment via focal adhesion (FA) in three dimensions (3-D) play a key role in dynamic biological events, such as tissue regeneration, wound healing, and cancer invasion. Recently, several methods for observing 3-D cell–extracellular matrix (ECM) interactions have been reported, lacking solid and quantitative analysis on the dynamics of the physical interaction between the cell and the ECM. We measured the submicron displacements of ECM deformation in 3-D due to protrusion-retraction dynamics during cell migration, using second-harmonic generation without labeling the matrix structures. We then quantitatively analyzed the mechanical deformation between the ECM and the cells based on spatiotemporal volumetric correlations. The greatest deformations within the collagen matrix were found to occur at sites of colocalization of the FA site-related proteins vinculin and actin, which confirms that FA sites play a critical role in living cells within the ECM as a point for adhesion, traction, and migration. We believe that this modality can be used in studies of cell–ECM interaction during angiogenesis, wound healing, and metastasis. [DOI: 10.1117/1.JBO.23.6.065001]

Keywords: second-harmonic generation; focal adhesion; matrix deformation; cell migration; digital volume correlation.

Paper 180040R received Jan. 18, 2018; accepted for publication May 14, 2018; published online Jun. 9, 2018.

1 Introduction

In many biological phenomena, such as development, wound healing, and even cancer metastasis, cells migrate in three-dimensional (3-D) space. Their movement is determined by the interaction between the cells and the environmental factors via adhesion sites. Cell–extracellular matrix (ECM) adhesions and cell–cell adhesions are known to regulate transcription and signaling pathways underlying cell migration, differentiation, proliferation, and morphogenesis.[1] This regulation indicates that mechanotransduction is an important factor in a variety of biological and biochemical reactions. However, classical chemical and biological assays do not enable measurement of mechanical deformations, especially at the single-cell level. Therefore, direct measurement of mechanical interaction is needed to find out the physical forces between the cell and the ECM.

In recent decades, several methods have been developed to monitor cell–substrate and cell–cell physical interactions during cell migration.[2–4] The methods enable measurement of ECM deformation and calculation of the traction force based on the deformation.[5] The displacements are generally quantified by embedding microsized fluorescent beads in a soft material, such as a polyethylene glycol or a polyacrylamide gel with a known elastic modulus. The displacement field of the particles together with the modulus is used to calculate the cellular forces.[6–8] This method has also been used to measure the interaction between cells and ECM in 3-D.[9–13] However, the force at the cell–ECM interface is difficult to compute accurately, because of the nonhomogeneity of ECM at the level of single cells. Furthermore, methods based on fluorescent beads generate errors or artifacts because of bead uptake by cells and the independent movement of the beads, unlike the actual motion of the gel. To overcome this limitation, many research groups have proposed methods for direct imaging of ECM structures. For example, ECM structural images can be seen with confocal microscopy by labeling the structure with fluorescent dyes.[14,15] Furthermore, the second-harmonic generation (SHG) microscope ensures collagen ECM imaging without labeling.[16–20]

Most studies in the field of label-free collagen imaging have focused on demonstrating the reliability of the results.[16,20,21] Although this method has been shown to be reliable, applications to biological studies at the scale of cells are still uncommon.

SHG microscopy facilitates imaging of biological materials with noncentrosymmetric properties, such as fibrous collagen or striated muscles, without staining.[18,22] SHG microscopy provides excellent imaging of collagen structure in the depth and is widely used for histological analysis.[22–26] In addition, digital volume correlation (DVC), a 3-D extension of digital image correlation technology,[8,9,27–29] facilitates the measurement of 3-D deformation with a high degree of accuracy.[8,9,21,30] DVC quantifies the field of displacement by computing the maximum correlation between two consecutive volume images.[9,29] Using

---

*Address all correspondence to: Yongdoo Park, E-mail: ydpark@kumc.ac.kr; Beop-Min Kim, E-mail: bmk515@korea.ac.kr

[†] These authors contributed equally to this work.

the combined techniques of SHG and DVC, it is possible to observe 3-D interactions of cells and the ECM in the collagen ECM without labeling.[16] The combination of SHG and DVC represents an intuitive and efficient method to measure 3-D deformation while maintaining an environment similar to the human body.[21,27,28,30–32]

In this study, we developed a system adopting SHG microscopy and DVC to monitor the deformation of collagen structures without fluorescent labeling in 3-D. We confirmed that the SHG monitoring system can be used to successfully measure 3-D matrix deformation and characterize cellular and matrix interactions during cell extrusion, traction, and retraction within the 3-D collagen matrix. Furthermore, we showed that matrix deformation is related to the focal adhesion (FA) site, which is a colocalization site of vinculin and the actin cytoskeleton. These results demonstrate the ability to quantitatively observe the physical interaction of cells with the surrounding ECM in 3-D, via the FA site.

2 Materials and Methods

2.1 *Cell Preparation*

Human mesenchymal stem cells (hMSCs; Lonza) were cultured and maintained in a regular 75T flask (SPL) with Dulbecco's modified Eagle's medium (Lonza) supplemented with 10% fetal bovine serum (Gibco) and 1% (v/v) penicillin and streptomycin (Gibco). The cells were stored in an incubator (Panasonic) at 37°C with 5% CO_2 and used until eighth passage. Fluorescence imaging of the cell body was performed by labeling the cells using calcein-AM (Thermo Fisher Scientific).

2.2 *Immunofluorescence Staining*

Immediately after the acquisition of SHG images, hMSCs were fixed with 4% paraformaldehyde (Biosesang; Korea) for over 1 h. The fixed cells were treated sequentially with 0.4% Triton X-100 (Triton X-100) and with 5% bovine serum albumin (Sigma-Aldrich) before staining. In this study, F-actin and vinculin were stained to explain not only filopodia contraction but also protrusion with deformation of the matrix based on the previous study.[33] The cells were stained with a vinculin antibody (hVIN-1; Sigma-Aldrich) diluted (1:200) within the microchannel device and incubated overnight at room temperature. The treated cells were washed five times using a 1× phosphate buffer solution with a 0.1% Tween-20 (PBST). An Alexa Fluor 568-conjugated antimouse IgG secondary antibody (1:200; Life Technologies), Alexa Fluor 488 phalloidin (1:200; Life Technologies), and Hoechst (33342; 1:3000; Life Technologies) were added and stored in the dark for 2 h. Finally, the stained sample was gently washed five times with PBST, and fluorescent images were obtained using a confocal microscope (LSM 800, Carl Zeiss). We identified colocalized areas of actin and vinculin by performing a Boolean (AND) operation between confocal fluorescent images of proteins, to find the FA sites.

2.3 *Collagen Gel Preparation*

Collagen gels were prepared by mixing collagen type I (rat tail tendon, 3.5 mg/mL; Corning) with 10× phosphate buffer saline (Gibco), deionized water, and 0.5 N NaOH to achieve a pH of 7.4. Collagen gels were prepared at concentrations of 0.5, 1.5, and 2.5 mg/mL to optimize DVC performance. The collagen gel with 2.5 mg/mL concentration was used for cellular experiments. In addition, hMSCs were mixed with the collagen solution at a concentration of 2×10^4 cells/mL to monitor the internal structural deformation of the collagen caused by cells. The prepolymerized collagen solution, including cells, was introduced into the microchannel device[34] and stored in a CO_2 incubator for gelation (40 min).

To acquire the image of beads embedded in collagen gel, 2% (volume/volume) fluorescent microbeads (0.2 μm, yellow-green, 2.5% aqueous suspension; Sigma-Aldrich) were uniformly mixed with the prepolymerized collagen solution.

2.4 *3-D Imaging via Microchannel Device Fabrication*

To maintain the quality and quantity of the collagen matrix, we used a microchannel device to load the collagen gel onto the channel and maintain its 3-D shape.[34] The device was fabricated using polydimethylsiloxane (PDMS; Sylgard 184 Silicone Elastomer, Dow Corning) on a patterned SU-8 silicon wafer manufactured by MicroChem, based on our own design. The PDMS device was cured at 80°C for 2 h. The microchannel in the device was treated with poly-D-lysine (PDL; Sigma-Aldrich) for over 4 h. The PDL-treated device was washed three times with third-order distilled water and stored overnight.

2.5 *Live Cell SHG Microscopy*

A schematic illustration of the SHG microscopy system used in this study is shown in Fig. 1(a). A mode-locked Ti:sapphire laser (Chameleon Ultra II, Coherent) with a central wavelength of 815 nm (temporal pulse width = 140 fs) was used as a light source. After adjusting the input polarization and power of the light with a half-wave plate and a polarizing beam splitter, the linear polarized state was adjusted to a circularly polarized state with a quarter-wave plate to generate optical axis-independent SHG over the imaging plane.[31] A pair of galvanometer mirrors (GM1 and GM2) was used with the image delivery lenses in a 4-f configuration to avoid off-axis scanning distortion. Another 4-f system between GM2 and an objective lens (OBJ; 60×, 0.9 NA, Olympus) was adopted as a beam expander, filling the back aperture of the OBJ to attain maximum numerical aperture. Two photomultiplier tubes (PMT; Hamamatsu) were used in a photon-counting mode for signal detection. PMT1 was used to detect the two-photon fluorescence from fluorescent-labeled beads or cells in the backward direction. PMT2 detected the SHG signal in the forward direction using a dichroic mirror (Semrock) in conjunction with a bandpass filter (Semrock) to exclude the excitation light. Axial scanning was performed via computer-controlled translation of the OBJ using an OBJ positioner (MIPOS 500, PiezoJena). Samples were prepared in an on-stage incubator (Live Cell Instruments) at a temperature of 37°C and 5% CO_2 concentration with humidity to maintain cell viability for long-term measurements. The microscopic images were captured at a pixel resolution of $512 \times 512 \times 200$ voxels, and the acquisition time interval was set to 30 min for 3 h.

2.6 *Preprocessing and Virtual Deformation of Volumetric Image and DVC Analysis*

Using a custom MATLAB™ (2016, MathWorks) script, the stacks of images obtained from each measurement were compared to remove unwanted focus or stage drift. To verify the

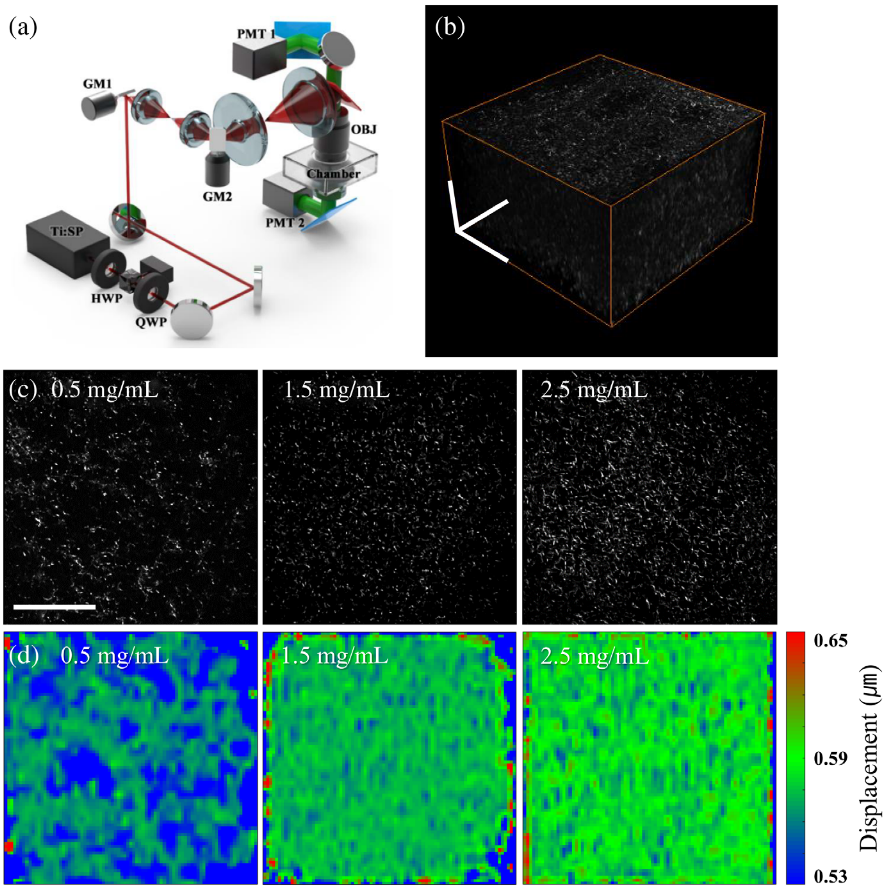

Fig. 1 SHG microscopy and effect of collagen concentration for validation of the DVC algorithm. (a) Schematic of SHG microscopy. HWP, half-wave plate; QWP, quarter-wave plate; GM1 and GM2, galvanometric mirrors; PMT1 and PMT2, photomultiplier tube; and OBJ, objective lens (60×). (b) Volume image of collagen type I gel at 2.5 mg/mL concentration using SHG microscopy. (c) Stacked SHG image of collagen type I. (d) Measured deformation map after 2.0 voxels (0.59 μm) of artificial deformation onto the x-axis at concentrations of 0.5, 1.5, and 2.5 mg/mL. Scale bars: 50 μm in (b) and (c).

validity of the DVC analysis with an SHG image, artificial deformation was applied to volumetric images of collagen gel and fluorescent beads obtained in the same laboratory setup. Deformations were applied for each spatial axis and measured via DVC analysis. The fast iterative digital volume correlation (FIDVC) algorithm was applied to measure the complex 3-D displacements.[30] FIDVC is an efficient method of DVC used for large nonlinear 3-D transformation fields. Because the reliability of DVC analysis depends on the subset size configuration, the configuration was carefully measured according to the specimen. In this system, a 10-voxel subset spacing and $40 \times 40 \times 40$ voxel subset size were used for the FIDVC analysis. To compute the cell-induced deformation, the image stack obtained immediately after the gelation was considered to be the zero-deformation state.

3 Results

3.1 *Verification of DVC Analysis using Collagen Gel Matrix*

We first demonstrated that SHG microscopy could visualize the collagen fiber structure in 3-D with a field of view (FOV) of $150 \times 150 \times 100$ μm, as shown in Fig. 1(b). Naturally, the reconstructed SHG images of collagen gel indicate that a higher concentration of collagen gel yielded a denser and more uniform structure. We tested three different collagen concentrations of 0.5, 1.5, and 2.5 mg/mL as shown in Fig. 1(c) left, middle, and right, respectively. Following measurement of the stack of images from each concentration of collagen gel, uniform translations (2.0 voxels; 0.59 μm) were applied for each stack, and the global deformation was estimated with DVC analysis. Figure 1(d) shows the displacement map for each concentration of the collagen gel. The mean values of deformation were 1.83 (0.54 μm), 1.92 (0.57 μm), and 1.96 (0.58 μm) voxels, and the standard deviations (SD) were 0.22 (0.07 μm), 0.15 (0.04 μm), and 0.09 (0.02 μm) voxels corresponding to 0.5, 1.5, and 2.5 mg/mL, respectively. The collagen gels with 2.5 mg/mL concentration show the closest value of deformation to an applied translation of 2.0 voxels (0.59 μm) and the smallest SD of 0.09 (0.02 μm). As a result, the collagen gel at 2.5 mg/mL facilitated the detection of deformation reliably with DVC analysis. Although a higher concentration of collagen gel yielded a finer and uniform matrix, a very high concentration of collagen gel tends to prohibit cellular motion.[32] Therefore, we used 2.5 mg/mL of collagen concentration in our study.

To verify the accuracy of the collagen gel deformation measurement using SHG microscopy, we compared the displacement based on two different correlation features: the fluorescent images of microbeads, a proven method for DVC analysis,[9] and SHG images of the collagen fibers. First, the microbead fluorescent images were captured simultaneously with SHG images of the collagen matrix structure. Then, translations were applied to both the microbead-based fluorescence and SHG images using a computer. Translations had magnitudes of 2, 4, and 6 voxels and were in each of the x-, y- (0.59, 1.18, and 1.77 μm), and z (1.0, 2.0, and 3.0 μm)-directions. DVC was used to compute the displacements by comparing translated image stacks to untranslated ones. For fluorescence and SHG images, the mean errors were 0.08 (0.024 μm) and 0.03 (0.008 μm) voxels, taken from the x-, y-, and z-directions. The z-axis error was slightly worse than that of the x- and y-axes, because the sampling resolution of the x- and y-axes was 0.29 μm, which was better than the 0.5 μm of the z-axis. Nevertheless, the mean errors in using DVC on SHG images are ~10 nm, which is smaller than the diameter of a collagen fibril (several hundred nanometers).[35] These results indicate that errors were negligible and that analysis of SHG images by DVC was reliable.

To compare the accuracy of DVC in the collagen matrix deformation induced by living cells (hMSC), we carried out the experiment using the same method as for the artificial deformation. Figure 2(b) (left) shows the magnitude of the 3-D deformation map using the conventional fluorescent beads method, and Fig. 2(b) (right) shows the map of the collagen gel (imaged with SHG) as a stack of xy-slices. The map of collagen deformation showed large displacements around the cells, located at the center of the imaging volume (square with dotted line; approximate cell size 30 μm), indicating cells pushing or pulling on the collagen fibers, as shown in Figs. 2(b) and 3. The measured deformation around the cell is shown as an inset in Fig. 2(c). The line profile of deformation around the dotted squared region for each modality is plotted as red and blue lines in Fig. 2(c). These data were acquired from a single xy-slide at a height of 25 μm from the bottom. The relative error of the measured deformation is calculated by dividing the magnitude of difference in deformation between beads and collagen by the magnitude of bead deformation. In this line profile of error, the mean value was 0.008, and SD was 0.027. The results of the two sets indicate almost identical deformation and appear to adequately describe the 3-D behavior of the cellular interaction with the surrounding physical environment. We repeated this experiment at five distinct times and obtained consistent results. The mean value of root mean square was 0.036 μm, and SD was 0.021 μm (data not shown).

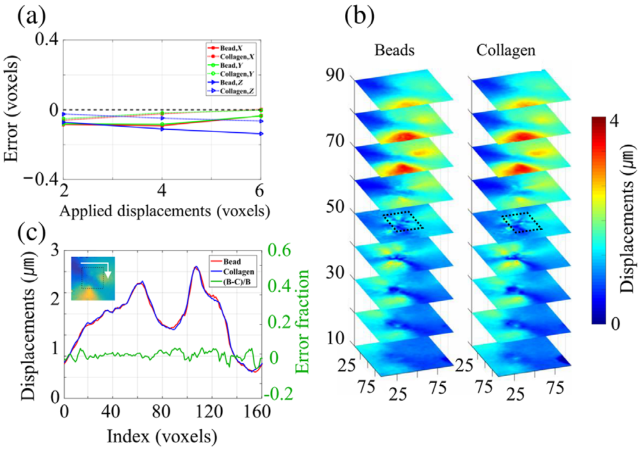

Fig. 2 Comparison of accuracy between fluorescent-beads- and SHG-collagen-based DVC algorithms. (a) Comparison of DVC results computed by fluorescent-bead images (solid line) and SHG-collagen images (dashed line) for each of the x- (red), y- (green), and z (blue)-axes. The error, or difference between the applied displacements and the measured displacements, was computed and plotted. (b) Cell-induced displacements measured via imaging of fluorescent beads (left) and collagen fibers (right). (c) Line profile of displacements along rectangular area (dotted line) of a single xy-slide (height = 25 μm) and its relative error.

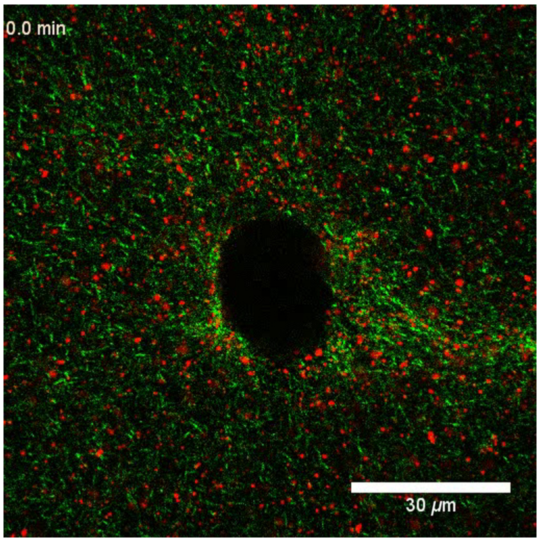

Fig. 3 Time-lapse video of fluorescent-bead-embedded collagen gel. Bead (red) and collagen gel (green) show displacements over a single xy-slide (Video 1, MPEG, 1.04 MB [URL: https://doi.org/10.1117/1.JBO.23.6.065001.1]).

3.2 *Quantifying 3-D Deformation of ECM using DVC Analysis*

Measurement of displacements in the collagen gel matrix facilitated the visualization of the 3-D cell–ECM interactions. Live cell images of hMSC within collagen gels were acquired with SHG microscopy and analyzed with DVC to compute the deformation. Five different samples were imaged and quantified for the matrix displacements. A representative case was plotted as a vector cone-plot map with the colors representing the magnitude of displacement, as shown in Fig. 4(a). The direction of the cone plot shows the displacements of the collagen matrix. Figures 4(b) and 4(c) are enlarged images of the orange- and green-dotted boxes in Fig. 4(a), which show displacement vectors surrounding either filopodia or the centroid of the cell body. Figures 4(b) and 4(c) show that the directions of deformation differ with each position of the cell. To investigate the deformations induced by the cell, the deformation of the collagen gel was computed as a function of distance from the cell surface. In addition, to analyze the deformation direction of cell–ECM, the cone-plot vectors of displacement were decomposed into either normal (N) or tangential (T) with respect to normal of the adjacent cell surface. Figure 4(b), which shows the protruding tip region, represents the magnitude of the deformation according to the distance from the cell surface, as shown in Fig. 4(d). At the collagen gel near the protruding tip of the cell, the magnitude of the N component was distributed more than the magnitude of the T component. Whereas the magnitude of deformation around the centroid of the cell is modest in

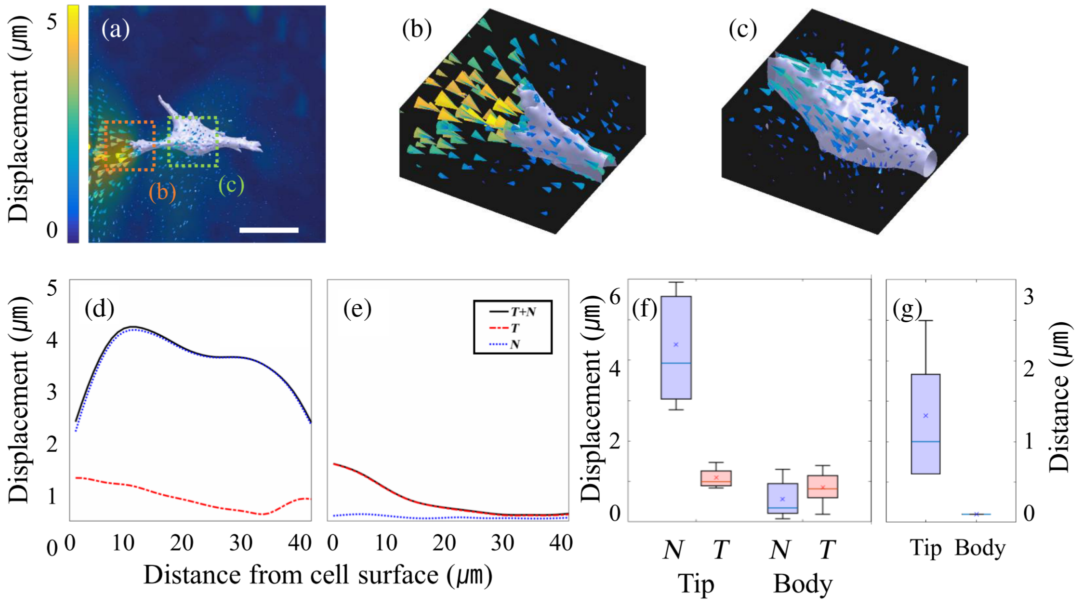

Fig. 4 Visualization of mechanical deformation between cell and ECM. (a) Cone plot of deformation during hMSC protrusion, (b) filopodia, and (c) centroid of cell body shows different aspects of deformation. (d) and (e) Magnitude of displacement as a function of the distance from the surface. The N and T components around the cell correspond to (b) and (c), respectively. (f) The box plot shows the magnitude of N and T near the tip and body of cells ($n = 5$). (g) The box plot shows the distance between the local maximum deformation and the cell surface ($n = 5$). Scale bars: 50 μm.

Fig. 4(c), most deformation arrows show T components, as shown in Fig. 4(e), suggesting that the cell pulls only the ECM around the cell toward the cell body via a protrusion, such as the one shown in Fig. 4(b). Figure 4(f) is a box plot of the mean magnitude near the tip and the body of cell ($n = 5$ for each case).

Interestingly, as shown in Fig. 4(d), the location of the maximum value of the displacement was not close to the tip of the protrusion, contrary to our expectations. In most cases, the maximum displacement occurred in a few tens of micrometers away from the cell membrane, which was consistent with the scaling laws in response to a nonlinear elastic material that predicts increase in displacement before decay with distance from cell surface.[36] Figure 4(g) is a box plot which represents the distance between the local maximum deformation and the cell surface ($n = 5$ for each case).

3.3 Decomposition of Displacement on the Cell Surface

To differentiate the type of mechanical stress applied from the cell surface, we compared the ratio of displacement vector components decomposed into N and T around its normal surface of the cell membrane. The ratio of the magnitudes of the two vector components was computed as

$$\text{ratio}(x,y,z) = \frac{|T(x,y,z)| - |N(x,y,z)|}{|T(x,y,z)| + |N(x,y,z)|}, \tag{1}$$

where T indicates the tangential component and N is the normal component of displacement. Equation (1) facilitates analysis of the directionality of applied stress from the cell surface; a value close to $+1$ indicates the presence of only displacements of tangential component and -1 values represent only normal components.

A typical image of a cell migrating is shown in Fig. 5(a), which has been selected from the four samples imaged. The cell migrated toward the lower right (marked as a yellow arrow) with protrusions in the collagen matrix. The deformation

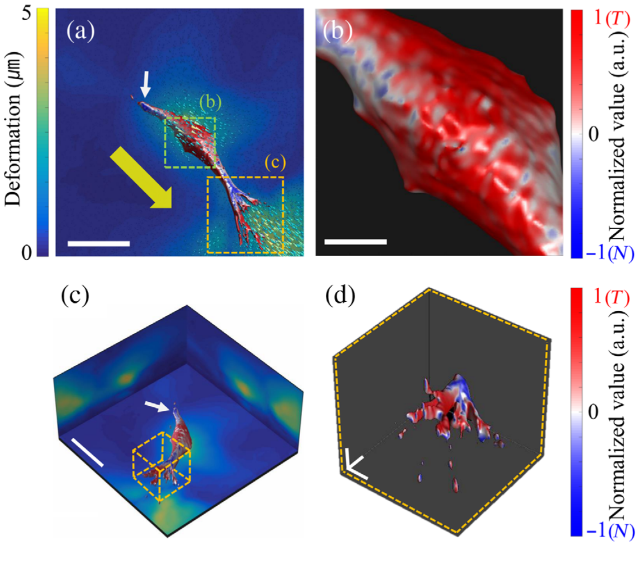

Fig. 5 Mapping over the cell surface by its deformation component with the cone plot of surrounding collagen matrix in 3-D. (a) Deformation around the cell using the cone plot and N and T components on the cell surface. The cell surface was patched with the ratio determined by Eq. (1). Red color denotes the tangential component, and blue represents the normal component. Yellow arrow denotes the direction of the cell migration and white arrow is the branch opposite to the protrusion direction. (b) Cropped FOV shows tangential deformations mostly occurring at the centroid of the migrating cell body. (c) In the protruding filopodia, normal components are located at the very tip, shown in blue color. Scale bar: 50 μm in (a), 10 μm in (b) and (c).

was plotted as a cone plot distributed around the cell body (green-dotted box) and at the end of the protrusion (orange-dotted box). As shown in the cone plot near the cell body, the deformation of the ECM occurred mostly in the direction of cell movement. We quantified this deformation by determining the ratio of N to T on the cell surface, shown in blue (-1) and red $(+1)$ color. As a result, the tangential components were clearly predominant, as shown in Fig. 5(b). On the other hand, the tip of the protrusion region (orange-dotted box) was remarkable, because the cone plot showed that the direction of deformation was distributed in the direction opposite to cell migration in Figs. 5(a) and 5(c). Figure 5(c) shows the ratio between the N and T components of the cell body surface and the projection of the deformation map for each orthogonal axis on the back plane of the imaging volume, which supports the idea that the FA sites form at the protrusion region, resulting in withdrawal of ECM of the collagen fiber toward the center of the cell body via focal points. Figure 5(d) is an enlarged image of the end of the protrusion facing the front of the migrating cell. As expected, the focal point confirms that the N components occur at the end of the cell. In addition, we realized that the N components were also distributed at the opposite sides of the protrusion region indicated by white arrows in Figs. 5(a) and 5(c). In this region, the branch does not grow forward. Instead, this area seems to support the protrusion of the opposite side.

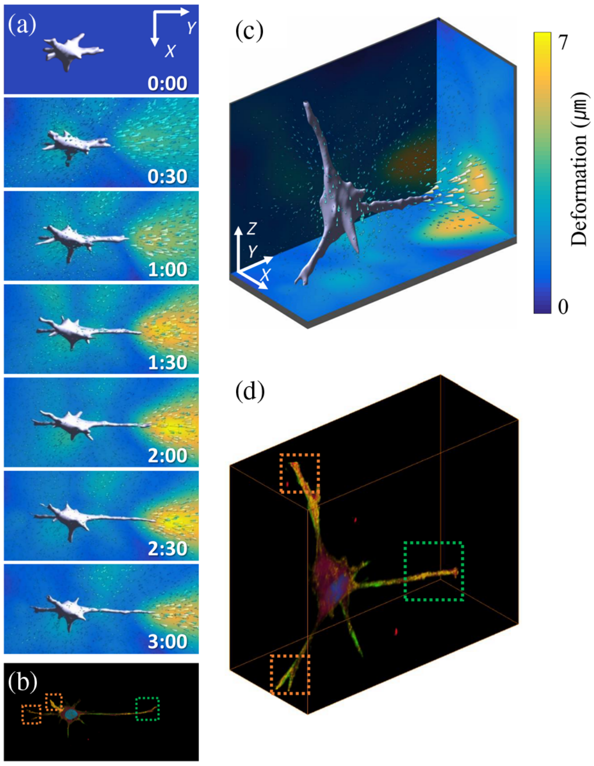

Fig. 6 Time-lapse observation of deformation in the hMSC. (a) Time series of protrusion show maximum strain area following the tip of protrusion. (b) Immunofluorescence image of hMSC immediately after time-lapse imaging. Green- and orange-squared regions show colocalization of vinculin and actin. Cell in the yellow-colored region denotes a colocalized area (blue: nucleus, green: actin, and red: vinculin. Scale bar: 20 μm, 30 min per frame). (c) and (d) represent bird's-eye views of (a) and (b).

3.4 *Identifying the Focal Adhesion Site Using Time-Lapse Imaging*

To investigate the relationship between deformation of the ECM and dynamics of the FAs, we performed time-lapse imaging at time intervals of 30 min for 3 h for four samples. Time-lapse imaging of cell migration during protrusion and retraction shows the step-by-step mechanical interaction between the cell and the surrounding ECM. A typical cone plot is shown in Fig. 6, where the cell shows the typical amoeboid shape and has branch-like protrusion regions within the FA site. In Fig. 6(a), the cell body has limited movement; however, the cell stretches protrusions toward the right over time. Also, deformation of the ECM at the tip of filopodia consistently occurred on the right side of the filopodia tip. The maximum deformation point of the ECM was located at the tip of the filopodia, as shown in Figs. 6(a) and 7. Immediately after time-lapse imaging, we detected the presence of FA by observing the distribution of actin and vinculin using the immunofluorescence assay from the four samples.[33] Vinculin, actin, and the nucleus are represented in red, green, and blue, respectively, as shown in Figs. 6(b) and 6(d). Thus, we confirmed the colocalization of actin and vinculin, regarded as FA, at the tip of the cell (in yellow color) with the deformation occurring consistently as shown in the green-dotted box in Fig. 6(b). However, the orange-dotted boxes also showed a strong colocalization of actin and vinculin in Fig. 6(b), without a strong deformation of ECM. Although these protrusion branches connected to the ECM through an FA site, they did not deform the ECM during the experiment. We confirmed this result as shown in the 3-D images in Figs. 6(c) and 6(d). In other words, the cells exerted sustained traction at

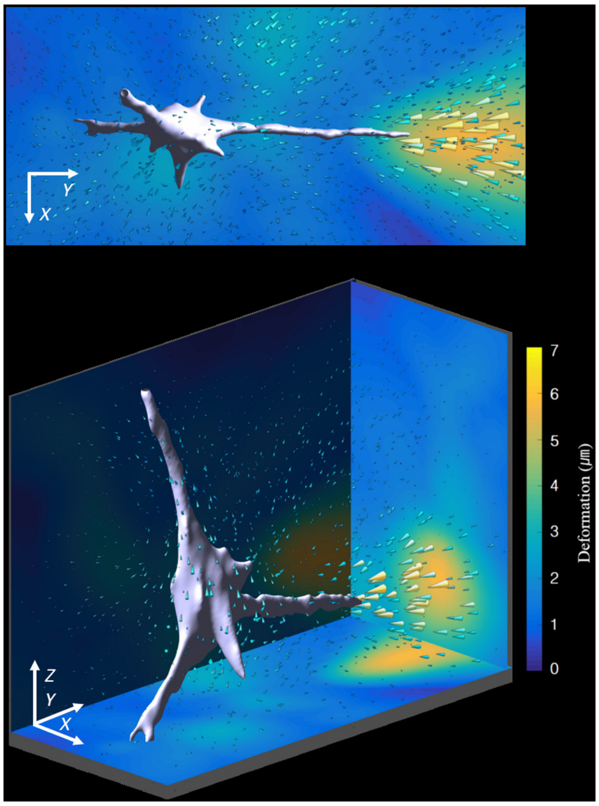

Fig. 7 Cone plot of deformation map based on time-lapse observations of hMSC in 3-D. Scale bar: 20 μm (Video 2, MPEG, 0.82 MB [URL: https://doi.org/10.1117/1.JBO.23.6.065001.2]).

the FA site in addition to extending their filopodia into the 3-D matrix.

4 Discussion and Conclusion

The accuracy of DVC analysis based on microbeads depends on the initial bead concentration in the matrix. In a similar manner, if the cells modify the collagen matrix by secreting or degrade the collagen, beads will not be located in the modified region of the collagen matrix. In this case, the concentration of beads decreased locally, which reduces the accuracy of the DVC analysis. Moreover, collagen fibers labelled with fluorophores alter the mechanical properties of the fiber due to photocrosslinking and photobleaching. By contrast, SHG does not entail optical excitation of collagen molecules and, therefore, does not alter the mechanical properties. The SHG microscopy system, which does not require labeling, is therefore an ideal method for observation of cell–ECM matrix interactions over a long time. Compared with these limitations, SHG yields significant results via direct reflection of the structural changes in collagen scaffold deformation resulting from interaction with cells.

DVC analysis allowed us to map the 3-D cell-induced displacements based on the volumetric images of the gel structure. In principle, it enabled computation of the stress tensor surrounding the cell.[10,11] However, even if the collagen gels were prepared under similar concentrations, the small differences in experimental conditions led to large differences in mechanical properties.[37,38] Furthermore, collagen gel itself is a heterogeneous and nonlinear material resulting from the fibrous structure.[11,39–41] Therefore, it is still a challenge to use mechanical properties of the collagen gel to calculate the stress in the matrix or traction at the cell–matrix interface. Several groups have begun to address this challenge by quantifying the relationship between collagen structure and mechanics[12,41–44] or by estimating the mechanical modulus of a collagen gel based on the image features, such as the diameter of each fiber.[45]

In this study, we developed a method using SHG microscopy to monitor the structural changes of collagen fibers induced by cells in a 3-D matrix. SHG has a good contrast, especially for collagen fibers. The analysis of the changing collagen structure using the SHG microscopy system and the DVC algorithm showed cellular interaction with ECM physically when the cells move within the 3-D structure. We were specifically interested in the deformation-focused areas related to the actin–vinculin colocalization site in filopodia as well as the tendency for the N components to distribute mainly on the cellular filopodia surface. Some of the FAs, identified by colocalization of actin and vinculin, showed no deformation in the surrounding ECM since these FA sites may not support the migration of cells, so the cells do not exhibit enough tension against the FA. However, more research is needed to confirm this speculation. In summary, this modality facilitates the observation of the dynamic interaction between cell and ECM, along with the dynamic changes of FA without the need for labeling as an approach for biological studies.

Studies investigating the relationship between ECM characteristics and cell migration are closely related to the understanding of the various biological phenomena, such as tissue regeneration, wound healing, and cancer metastasis.[10,46,47] Therefore, monitoring of not only cells but also the surrounding ECM provides insights compared with conventional biological analysis and provides an approach to elucidating the 3-D remodeling of biological tissues.

Disclosures

All the authors declare the absence of any conflicts of interest.

Acknowledgments

This work was supported by the National Research Foundation of Korea (Nos. 2014R1A2A1A11051879, 2017R1A6A3A11031083, and 2015H1A2A1030048) and the Ministry of Health and Welfare Grant (No. HI13C1501) funded by the Korean government.

References

1. P. Roca-Cusachs, V. Conte, and X. Trepat, "Quantifying forces in cell biology," *Nat. Cell Biol.* **19**, 742–751 (2017).
2. A. Harris, P. Wild, and D. Stopak, "Silicone rubber substrata: a new wrinkle in the study of cell locomotion," *Science* **208**(4440), 177–179 (1980).
3. M. P. Sheetz, D. P. Felsenfeld, and C. G. Galbraith, "Cell migration: regulation of force on extracellular-matrix-integrin complexes," *Trends Cell Biol.* **8**(2), 51–54 (1998).
4. N. Q. Balaban et al., "Force and focal adhesion assembly: a close relationship studied using elastic micropatterned substrates," *Nat. Cell Biol.* **3**(5), 466–472 (2001).
5. R. J. Pelham and Y.-l. Wang, "High resolution detection of mechanical forces exerted by locomoting fibroblasts on the substrate," *Mol. Biol. Cell* **10**(4), 935–945 (1999).
6. W. R. Legant et al., "Measurement of mechanical tractions exerted by cells within three-dimensional matrices," *Nat. Methods* **7**(12), 969–971 (2010).
7. S. S. Hur et al., "Live cells exert 3-dimensional traction forces on their substrata," *Cell. Mol. Bioeng.* **2**(3), 425–436 (2009).
8. S. A. Maskarinec et al., "Quantifying cellular traction forces in three dimensions," *Proc. Natl. Acad. Sci. U. S. A.* **106**(52), 22108–22113 (2009).
9. C. Franck et al., "Three-dimensional full-field measurements of large deformations in soft materials using confocal microscopy and digital volume correlation," *Exp. Mech.* **47**(3), 427–438 (2007).
10. C. Franck et al., "Three-dimensional traction force microscopy: a new tool for quantifying cell–matrix interactions," *PLoS One* **6**(3), e17833 (2011).
11. N. Gjorevski and C. M. Nelson, "Mapping of mechanical strains and stresses around quiescent engineered three-dimensional epithelial tissues," *Biophys. J.* **103**(1), 152–162 (2012).
12. T. M. Koch et al., "3D traction forces in cancer cell invasion," *PLoS One* **7**(3), e33476 (2012).
13. A. Lesman et al., "Contractile forces regulate cell division in three-dimensional environments," *J. Cell Biol.* **205**(2), 155–162 (2014).
14. P. Friedl and E. B. Bröcker, "The biology of cell locomotion within three-dimensional extracellular matrix," *Cell. Mol. Life Sci.* **57**(1), 41–64 (2000).
15. J. Kim et al., "Three-dimensional reflectance traction microscopy," *PLoS One* **11**(6), e0156797 (2016).
16. A. Jorge-Peñas et al., "3D full-field quantification of cell-induced large deformations in fibrillar biomaterials by combining non-rigid image registration with label-free second harmonic generation," *Biomaterials* **136**(Suppl. C), 86–97 (2017).
17. J. Notbohm et al., "Quantifying cell-induced matrix deformation in three dimensions based on imaging matrix fibers," *Integr. Biol.* **7**(10), 1186–1195 (2015).
18. B.-M. Kim, J. Eichler, and L. B. Da Silva, "Frequency doubling of ultrashort laser pulses in biological tissues," *Appl. Opt.* **38**(34), 7145–7150 (1999).
19. K. Sanen et al., "Label-free mapping of microstructural organisation in self-aligning cellular collagen hydrogels using image correlation spectroscopy," *Acta Biomater.* **30**, 258–264 (2016).
20. D. E. Midgett et al., "The pressure-induced deformation response of the human lamina cribrosa: analysis of regional variations," *Acta Biomater.* **53**(Suppl. C), 123–139 (2017).

21. D. E. Midgett et al., "Inflation test of the human optic nerve head using digital volume correlation," in *Mechanics of Biological Systems and Materials*, S. A. Tekalur, P. Zavattieri, and C. S. Korach, Eds., pp. 7–15, Springer International Publishing, Cham (2016).
22. T. Hompland et al., "Second-harmonic generation in collagen as a potential cancer diagnostic parameter," *J. Biomed. Opt.* **13**(5), 054050 (2008).
23. L. Moreaux, O. Sandre, and J. Mertz, "Membrane imaging by second-harmonic generation microscopy," *J. Opt. Soc. Am. B* **17**(10), 1685–1694 (2000).
24. P. Friedl et al., "Biological second and third harmonic generation microscopy," *Curr. Protoc. Cell Biol.* **4**, 4.15 (2007). (2001).
25. P. J. Campagnola et al., "Three-dimensional high-resolution second-harmonic generation imaging of endogenous structural proteins in biological tissues," *Biophys. J.* **82**(1), 493–508 (2002).
26. S.-J. Lin et al., "Evaluating cutaneous photoaging by use of multiphoton fluorescence and second-harmonic generation microscopy," *Opt. Lett.* **30**(17), 2275–2277 (2005).
27. M. Palanca, G. Tozzi, and L. Cristofolini, "The use of digital image correlation in the biomechanical area: a review," *Int. Biomech.* **3**(1), 1–21 (2016).
28. A. Saraswathibhatla and J. Notbohm, "Applications of DIC in the mechanics of collective cell migration," in *International Digital Imaging Correlation Society*, M. Sutton and P. L. Reu, Eds., pp. 51–53, Springer International Publishing, Cham (2017).
29. B. A. Roeder et al., "Local, three-dimensional strain measurements within largely deformed extracellular matrix constructs," *J. Biomech. Eng.* **126**(6), 699–708 (2005).
30. E. Bar-Kochba et al., "A fast iterative digital volume correlation algorithm for large deformations," *Exp. Mech.* **55**(1), 261–274 (2015).
31. X. Chen et al., "Second harmonic generation microscopy for quantitative analysis of collagen fibrillar structure," *Nat. Protoc.* **7**(4), 654–669 (2012).
32. K. Watanabe et al., "Establishment of three-dimensional culture of neural stem/progenitor cells in collagen type-1 gel," *Restor. Neurol. Neurosci.* **25**(2), 109–117 (2007).
33. H. Jang et al., "Homogenizing cellular tension by hepatocyte growth factor in expanding epithelial monolayer," *Sci. Rep.* **7**, 45844 (2017).
34. S. Park et al., "Directional migration of mesenchymal stem cells under an SDF-1α gradient on a microfluidic device," *PLoS One* **12**(9), e0184595 (2017).
35. R. Parenteau-Bareil, R. Gauvin, and F. Berthod, "Collagen-based biomaterials for tissue engineering applications," *Materials* **3**(3), 1863–1887 (2010).
36. Y. Shokef and S. A. Safran, "Scaling laws for the response of nonlinear elastic media with implications for cell mechanics," *Phys. Rev. Lett.* **108**(17), 178103 (2012).
37. B. Burkel et al., "Preparation of 3D collagen gels and microchannels for the study of 3D interactions in vivo," *J. Visualized Exp.* (111), e53989 (2016).
38. E. Gentleman et al., "Mechanical characterization of collagen fibers and scaffolds for tissue engineering," *Biomaterials* **24**(21), 3805–3813 (2003).
39. H. Rich et al., "Effects of photochemical riboflavin-mediated crosslinks on the physical properties of collagen constructs and fibrils," *J. Mater. Sci. Mater. Med.* **25**(1), 11–21 (2014).
40. D. A. Head, A. J. Levine, and F. C. MacKintosh, "Distinct regimes of elastic response and deformation modes of cross-linked cytoskeletal and semiflexible polymer networks," *Phys. Rev. E* **68**(6), 061907 (2003).
41. L. Long et al., "Heterogeneous force network in 3D cellularized collagen networks," *Phys. Biol.* **13**(6), 066001 (2016).
42. B. Burkel and J. Notbohm, "Mechanical response of collagen networks to nonuniform microscale loads," *Soft Matter* **13**(34), 5749–5758 (2017).
43. J. Yang and T. Salvatore, "Quantitative characterization of the microstructure and transport properties of biopolymer networks," *Phys. Biol.* **9**(3), 036009 (2012).
44. J. Steinwachs et al., "Three-dimensional force microscopy of cells in biopolymer networks," *Nat. Methods* **13**(2), 171–176 (2016).
45. Y.-l. Yang, L. M. Leone, and L. J. Kaufman, "Elastic moduli of collagen gels can be predicted from two-dimensional confocal microscopy," *Biophys. J.* **97**(7), 2051–2060 (2009).
46. X. Trepat et al., "Physical forces during collective cell migration," *Nat. Phys.* **5**(6), 426–430 (2009).
47. A. Haeger et al., "Collective cell migration: guidance principles and hierarchies," *Trends Cell Biol.* **25**(9), 556–566 (2015).

Biographies for the authors are not available.